Rapid Communications

Multipole fluctuation theory for heavy fermion systems: Application to multipole orders in CeB_6

Rina Tazai and Hiroshi Kontani
Department of Physics, Nagoya University, Furo-cho, Nagoya 464-8602, Japan

(Received 15 January 2019; revised manuscript received 20 November 2019; published 6 December 2019)

In heavy fermion systems, the emergence of rich phenomena, such as hidden orders and superconductivities, is made possible by multipole degrees of freedom. However, many of them remain unsolved since the origin of the higher-rank multipole interaction is not well understood. Among these issues, we focus on the quadrupole order in CeB_6, which is a famous multipolar heavy fermion system that has been actively studied for decades. We analyze the multiorbital periodic Anderson model for CeB_6, and find that magnetic, quadrupole, and octupole fluctuations all develop cooperatively due to the strong intermultipole coupling given by higher-order many-body effects, called vertex corrections. It is found that the antiferroquadrupole order in CeB_6 is driven by the interference between magnetic-multipole fluctuations. The discovered intermultipole coupling mechanism is a potential origin of numerous hidden orders in various heavy fermion systems.

DOI: 10.1103/PhysRevB.100.241103

Heavy fermion (HF) systems are a very interesting platform of exotic electronic states induced by a strong Coulomb interaction and spin-orbit interaction (SOI) on the f electrons. Magnetic fluctuations cause interesting quantum critical phenomena and superconductivity [1–8]. In addition, higher-rank multipole operators are also active owing to the strong SOI of f electrons. For this reason, various interesting multipole order and fluctuations, which are absent in transition metal oxides, emerge in HF systems. One of the most famous examples is the multipole order in CeB_6: The antiferroquadrupole order with $\boldsymbol{q} = (\pi, \pi, \pi)$ occurs at $T_Q = 3.2$ K, and a magnetic order appears at $T_N = 2.4$ K [9–12]. In addition, the antiferrooctupole order is stabilized under a weak magnetic field [13–16]. Thus, various ranks of multipole orders appear simultaneously in the phase diagram of CeB_6. This fact indicates that different multipoles are strongly entangled, which would be universal in HF systems.

Up to now, multipole orders in CeB_6 have been studied actively based on the localized f-multipole models [13–19]. Recent angle-resolved photoemission spectroscopy (ARPES) and neutron inelastic scattering measurements of CeB_6, in addition to the x dependence of the de Haas–van Alphen (dHvA) effect for $Ce_xLa_{1-x}B_6$, revealed that the f electron has an itinerant nature above $T \sim T_Q$ [20–25]. These findings indicate that the itinerant picture is a fruitful starting point to understand the multipole physics of CeB_6. Therefore, in this Rapid Communication, we study this longstanding problem based on the periodic Anderson model (PAM), in which the f electrons hybridize with conduction electrons and form itinerant heavy quasiparticles.

If we apply the random-phase approximation (RPA) for the PAM, however, quadrupole order cannot be obtained. In fact, only odd-rank (=magnetic) multipole fluctuations develop, whereas even-rank (=electric) multipole ones remain small in the RPA [24,26,27]. This fact reveals the importance of vertex corrections (VCs), which represent the many-body effects ignored in the RPA. The Fermi-liquid approach has succeeded in explaining phase diagrams in HF materials, such as CeB_6 [24], URu_2Si_2 [26], and $CeCu_2Si_2$ [27]. Although HF systems have a large Coulomb interaction, it is renormalized by the renormalization factor z as zU. Since $z \ll 1$ in HF systems, the Fermi-liquid theory is still applicable even in the presence of strong Coulomb interactions. The lowest-order VC with respect to fluctuations, called a Maki-Thompson (MT)-type VC, gives a rank-5 multipole order in URu_2Si_2 [26]. However, the MT-VC does not magnify even-rank multipole fluctuations. Thus, the microscopic origin of the quadrupole order, which frequently appears in various compounds, is still unsolved. CeB_6 is a suitable platform to construct a theory of multipole order in HF systems.

Recently, it was revealed that an Aslamazov-Larkin (AL) VC, which is of higher order than MT-VC, gives a nematic orbital order in Fe-based superconductors [28–30]. Analytically, AL-VC is proportional to ξ^{4-d} in d-dimension systems at a fixed T, where ξ is the magnetic correlation length. Therefore, AL-VC plays an important role near the magnetic quantum criticality. We stress that the significance of AL-VC is confirmed by functional-renormalization-group (fRG) studies, by which we can consider higher-order VC in an unbiased way [31–37].

We recently studied the role of VCs for electron-phonon (el-ph) interactions beyond the Migdal approximation, and found that the weak phonon-mediated attractive interaction is strongly magnified by AL-type VCs [38]. Based on this mechanism, we explained recently the fully gapped s-wave pairing state in $CeCu_2Si_2$ [27]. This fact strongly indicates the significance of AL-VC for multipole susceptibilities in HF systems.

In this Rapid Communication, we study the mechanism of the quadrupole order in CeB_6 based on the itinerant f-electron picture, by considering the AL-VC for multipole susceptibilities. For this purpose, we introduced an effective PAM for CeB_6 with a Γ_8 quartet f-orbital basis. Both ferro- and antiferromagnetic and octupole fluctuations are induced by Fermi-surface nesting, consistent with recent neutron experiments. Then, antiferroquadrupole (O_{xy}) order is induced

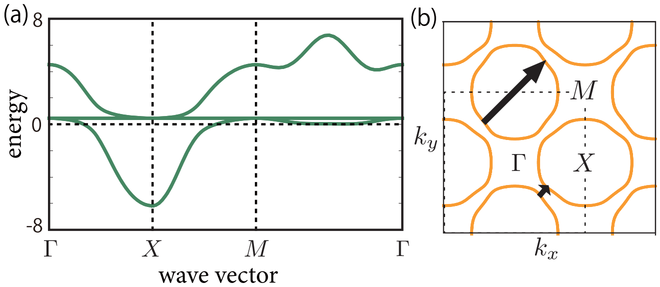

FIG. 1. (a) Band dispersion and (b) Fermi surfaces of the present model. Major nesting vectors are shown.

by the interference between different magnetic multipole fluctuations. The present multipole fluctuation theory with introducing AL-VC will be applicable for various HF systems.

Here, we introduce a two-dimensional PAM as an effective model for CeB_6. For f-electron states, we consider the Γ_8 quartet in $J = 5/2$ space due to the strong SOI [13],

$$|f_1\Sigma\rangle = \sqrt{\frac{5}{6}}\left|\mp\frac{5}{2}\right\rangle + \sqrt{\frac{1}{6}}\left|\pm\frac{3}{2}\right\rangle, \qquad |f_2\Sigma\rangle = \left|\mp\frac{1}{2}\right\rangle, \quad (1)$$

where $\Sigma = \pm$ is the pseudospin of the f_l orbital ($l = 1, 2$). The kinetic term is given by $\hat{H}_0 = \sum_{k\sigma} \epsilon_k c^\dagger_{k\sigma} c_{k\sigma} + \sum_{kl\sigma} E_f f^\dagger_{kl\sigma} f_{kl\sigma} + \sum_{kl\sigma} (V^*_{kl\sigma} f^\dagger_{kl\sigma} c_{k\sigma} + \mathrm{H.c.})$, where $c^\dagger_{k\sigma}$ is a creation operator for the s electron with momentum $\boldsymbol{k}$ and spin σ on the Ce ion. $\epsilon_{\boldsymbol{k}}$ is the conduction-band dispersion, which we explain in Supplemental Material (SM) A [39]. $f^\dagger_{\boldsymbol{k}l\Sigma}$ is a creation operator for the f electron with $\boldsymbol{k}$, orbital l, and pseudospin Σ. $V_{\boldsymbol{k}l\sigma}$ is the s-f hybridization term between the nearest Ce cites. In the two-dimensional model, the pseudospin and s-electron spin are conserved ($\sigma = \Sigma$) in the s-f mixing [27]. Using the tight-binding method [40], $V_{\boldsymbol{k}l\sigma}$ is given as

$$V_{\boldsymbol{k}f_l\uparrow} = -A_l t_{sf}[\sin k_y + (-1)^l i \sin k_x], \quad (2)$$

and $V_{\boldsymbol{k}f_l\downarrow} = -V^*_{\boldsymbol{k}f_l\uparrow}$. We set $A_l = \sqrt{18/14}$, and give a detailed explanation of $V_{\boldsymbol{k}l\sigma}$ in SM A [39]. Hereafter, we set $2|t^1_{ss}| = 1$ as the energy unit, and put $t_{sf} = 0.78$, $E_f = -2.0$, $T = 0.01$, and $\mu = -2.45$. Then, the $f(s)$-electron number is $n_f = 0.58$ ($n_s = 0.69$). We comment that n_f increases if we put the level of E_f lower under the constraint $n_f + n_c = \mathrm{const.}$ By this procedure, our main results will not change since the shape of the Fermi surface is essentially unchanged.

Figure 1(a) shows the band structure of PAM. The lowest band crosses the Fermi level ($\epsilon = 0$). Since $W_D \sim 5$ eV in CeB_6 [20,21,41,42], $2|t^1_{ss}|(=1)$ corresponds to $\sim$0.5 eV. The bandwidth of the itinerant f electron is $W^{qp}_D \sim |V| \sim 1$. The Fermi surfaces shown in Fig. 1(b) are composed of large ellipsoid electron pockets around the X, Y points, consistently with recent ARPES studies [20,21].

We also introduce the Coulomb interaction term $\hat{H}_U = u\hat{H}^0_U$. Here, $\hat{H}^0_U = \frac{1}{4}\sum_{LL'MM'} U^0_{L,L';M,M'} f^\dagger_L f_{L'} f_M f^\dagger_{M'}$, where $L = (l, \sigma)$ and $M = (m, \rho)$. $\hat{U}^0$ is the normalized Coulomb interaction for the Ce ion; the maximum element of $\hat{U}^0$ is set to unity. A detailed explanation is given in Ref. [27] and in SM A [39].

TABLE I. IRs and 16-type active multipole operators of the D_{4h} point group. The operator with rank k corresponds to 2^k-pole.

IR (Γ)	Rank (k)	Operator ($\hat{Q}$)	IR in H_z
Γ_1^+	0	$\hat{1}$	Γ_1
	2	$\hat{O}_{20}$	
Γ_3^+	2	$\hat{O}_{22}$	Γ_3
Γ_4^+	2	$\hat{O}_{xy}$	Γ_4
Γ_5^+	2	$\hat{O}_{yz}, \hat{O}_{zx}$	Γ_5
Γ_2^-	1	$\hat{J}_z$	Γ_1
	3	$\hat{T}_{z\alpha}$	
Γ_3^-	3	$\hat{T}_{xyz}$	Γ_4
Γ_4^-	3	$\hat{T}_{z\beta}$	Γ_3
Γ_5^-	1	$\hat{J}_x, \hat{J}_y$	Γ_5
	3	$\hat{T}_{x\alpha}, \hat{T}_{y\alpha}$	
	3	$\hat{T}_{x\beta}, \hat{T}_{y\beta}$	

In the present Γ_8 quartet model, there are 16-type active multipole operators up to rank 3: monopole, dipole (rank 1), quadrupole (rank 2), octupole (rank 3) momenta. The table of irreducible representations (IRs) for the D_{4h} two-dimensional model is shown in Table I [26]. An even-rank (odd-rank) operator corresponds to an electric (magnetic) multipole operator. The 4×4 matrix form of each operator $\hat{Q}$ is shown in SM B [39].

Here, we calculate the f-electron susceptibility. The bare irreducible susceptibility is given by $\chi^0_{\alpha,\beta}(q) = -T\sum_k G^f_{LM}(k+q) G^f_{M'L'}(k)$, where $q \equiv (\boldsymbol{q}, \omega_n) = (\boldsymbol{q}, 2j\pi T)$, $\alpha \equiv (L, L')$, and $\beta \equiv (M, M')$. Here, α, β takes 1–16, and $\hat{G}^f$ is the Green's function without self-energy [27]. We also consider the VCs due to AL and MT terms, $\hat{X}^{\mathrm{AL+MT}}$, which we will explain later. Then, f-electron susceptibility is given as

$$\hat{\chi}(q) = \hat{\phi}(q)[\hat{1} - u\hat{U}^0\hat{\phi}(q)]^{-1}, \quad (3)$$

where $\hat{\phi}(q) = \hat{\chi}^0(q) + \hat{X}^{\mathrm{AL+MT}}(q)$ is the irreducible susceptibility including the VCs in the 16×16 matrix form.

Here, we consider the following eigenequation,

$$u\hat{U}^0\hat{\phi}(\boldsymbol{q}, 0)\vec{w}^\Gamma(\boldsymbol{q}) = \alpha^\Gamma(\boldsymbol{q})\vec{w}^\Gamma(\boldsymbol{q}). \quad (4)$$

When the eigenvector is expressed as $\vec{w}^\Gamma(\boldsymbol{q}) = \sum_{Q\in\Gamma} Z^Q(\boldsymbol{q})\vec{Q}$, the maximum of the eigenvalue $\alpha^\Gamma(\boldsymbol{q})$ gives the Stoner factor for IR Γ, $\alpha^\Gamma = \max_{\boldsymbol{q}}\{\alpha^\Gamma(\boldsymbol{q})\}$. Here, $\vec{Q}$ is a 16×1 vector defined as $(\vec{Q})_\alpha = (\hat{Q})_{L,L'}$ and $Z^Q(\boldsymbol{q})$ is a real coefficient. The Γ-channel multipole order appears when $\alpha^\Gamma \geqslant 1$. The inner product $(\vec{Q})^\dagger\vec{Q}'$ is unity for $Q = Q'$. It is zero when Q and Q' belong to different IRs, whereas it is not always zero when $Q \neq Q'$ belong to the same IR [27,39]. We introduce the magnetic (electric) Stoner factor as $\alpha^{\mathrm{mag(el)}} = \max_n\{\alpha^{\Gamma_n^{-(+)}}\}$.

Using $\vec{Q}$, the multipole susceptibility is given by

$$\chi^{Q,Q'}(q) = (\vec{Q})^\dagger\hat{\chi}(q)\vec{Q}'. \quad (5)$$

First, we show the numerical results by the RPA, given as $X^{\mathrm{AL+MT}} = 0$. Figure 2 shows the obtained susceptibilities $\chi^Q(\boldsymbol{q}, 0) \equiv \chi^{Q,Q}(\boldsymbol{q}, 0)$ at $u = 1.08$ ($\alpha^{\mathrm{mag}} = 0.9$). In the RPA,

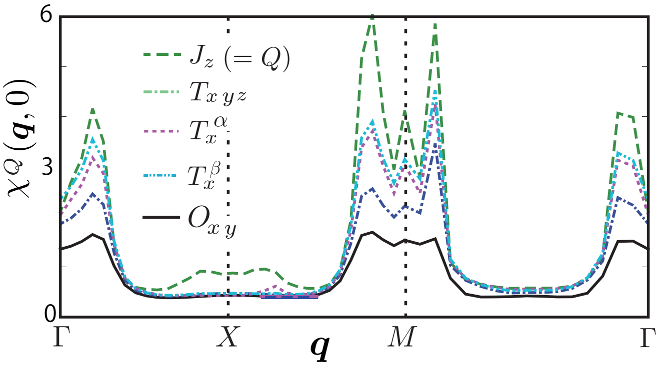

FIG. 2. Obtained multipole susceptibilities by the RPA. The peak positions correspond to the nesting vectors in Fig. 1(b). Note that $\chi^{O_{xy}} \neq \chi^{O_{xz(yz)}}$ in the present 2D model; see SM [39].

χ^{J_z} is the most largest. Second, $\chi^{T_\nu^\beta}$, $\chi^{T_\nu^\alpha} (\nu = x, y)$ and $\chi^{T_{xyz}}$ are also enlarged. $\chi^{J_z}(\boldsymbol{q}, 0)$ has a peak value at $\boldsymbol{q} \approx \boldsymbol{0}$ and $\boldsymbol{q} \approx \boldsymbol{Q} \equiv (\pi, \pi)$, which is consistent with the inelastic neutron scattering that reports strong ferromagnetic and antiferromagnetic $[\boldsymbol{q} = (\pi, \pi, \pi), (\pi, \pi, 0)]$ fluctuations above T_N [23,43]. Therefore, the present two-dimensional PAM is reliable.

On the other hand, the RPA quadrupole susceptibility remains small. To understand this result, we examine the (Q, Q') component of the normalized Coulomb interaction,

$$U_0^{Q,Q'} = (\vec{Q})^\dagger \hat{U}^0 \vec{Q}'. \tag{6}$$

Table II shows the diagonal component $U_0^Q \equiv U_0^{Q,Q}$. Since U_0^Q for the quadrupole channels is much smaller than that for the dipole and octupole channels, the quadrupole susceptibilities are small within the RPA.

From now on, we introduce the VCs due to AL and MT terms. Diagrams of these VCs are shown in Fig. 3(a). For example, the AL1 term is given as

$$X_{\alpha\beta}^{\mathrm{AL1}}(q) = \frac{T}{2} \sum_{\alpha'\alpha''\beta'\beta''} \Lambda_{\alpha'\beta''}^{\alpha}(q, p) V_{\alpha'\beta'}(p - q) \times V_{\alpha''\beta''}(p) \Lambda_{\beta'\alpha''}^{\beta *}(\bar{q}, \bar{p}), \tag{7}$$

where $p \equiv (\boldsymbol{p}, \omega_m)$, $\bar{p} \equiv (\boldsymbol{p}, -\omega_m)$, and $\hat{V}(q) \equiv u^2 \hat{U}^0 \hat{\chi}(q) \hat{U}^0 + u \hat{U}^0$ is the dressed interaction given by the RPA. The three-point vertex is given as

$$\Lambda_{ABCD}^{EF}(q, p) \equiv -T \sum_k G_{AF}^f(k - q) G_{EC}^f(k) G_{DB}^f(k - p). \tag{8}$$

Other VCs are explained in SM C [39].

Figures 3(b) and 3(c) show the obtained quadrupole susceptibility by including MT- and AL-VCs. In contrast to the RPA result, the obtained $\chi^{O_{xy}}(\boldsymbol{q}, 0)$ is strongly enhanced at $\boldsymbol{q} = \boldsymbol{Q}$ and $\boldsymbol{q} = \boldsymbol{0}$, and becomes the largest of all χ^Q. This enhancement originates from the AL terms, whereas the MT term is very small as we show in SM C [39]. The obtained $\chi^{O_{xy}}(\boldsymbol{q}, 0)$ has the highest peak at $\boldsymbol{q} = \boldsymbol{Q}$, consistent with the antiferro-O_{xy} order in CeB_6. Moreover, the second highest peak of $\chi^{O_{xy}}(\boldsymbol{q}, 0)$ at $\boldsymbol{q} = \boldsymbol{0}$ explains the softening of shear modulus C_{44} in CeB_6 [10]. We show other quadrupole susceptibilities in SM C [39]. To summarize, the obtained strong enhancements of $\chi^{O_{xy}}(\boldsymbol{q}, 0)$ and $\chi^{J_z}(\boldsymbol{q}, 0)$ at both $\boldsymbol{q} = \boldsymbol{Q}$ and $\boldsymbol{q} = \boldsymbol{0}$ reproduce the key experimental results of CeB_6.

Next, we explain that the O_{xy} quadrupole order is derived from the interference between magnetic multipole fluctuations. For this purpose, we analyze the total AL term $\hat{X} \equiv \hat{X}^{\mathrm{AL1}} + \hat{X}^{\mathrm{AL2}}$ for the O_{xy} channel defined as

$$X_{O_{xy}}(q) \equiv (\vec{O}_{xy})^\dagger \hat{X}(q) \vec{O}_{xy}, \tag{9}$$

where $\hat{X} \equiv \hat{X}^{\mathrm{AL1}} + \hat{X}^{\mathrm{AL2}}$. The Stoner factor for the $O_{xy}(=\Gamma_4^+)$ channel is proportional to $u U_0^{O_{xy}} \phi_{O_{xy}}(q)$, where $\phi_{O_{xy}}(q) \equiv (\vec{O}_{xy})^\dagger \hat{\phi}(q) \vec{O}_{xy}$. Therefore, $X_{O_{xy}}(q)$ (>0) works as the enhancement factor of O_{xy} susceptibility.

TABLE II. Normalized Coulomb interaction U_0^Q. $U_0^{Q,Q'} = 0$ for $Q \neq Q'$ except for $U_0^{J_\mu, T_\mu^\alpha} = 0.58$ $(\mu = x, y, z)$.

Q	1	$O_{20(22)}$	$O_{xy(yz,zx)}$	T_{xyz}	$J_{z(x,y)}$	$T_{z(x,y)}^\alpha$	$T_{z(x,y)}^\beta$
U_0^Q	−2.4	0.50	0.63	0.81	1.03	0.94	0.94

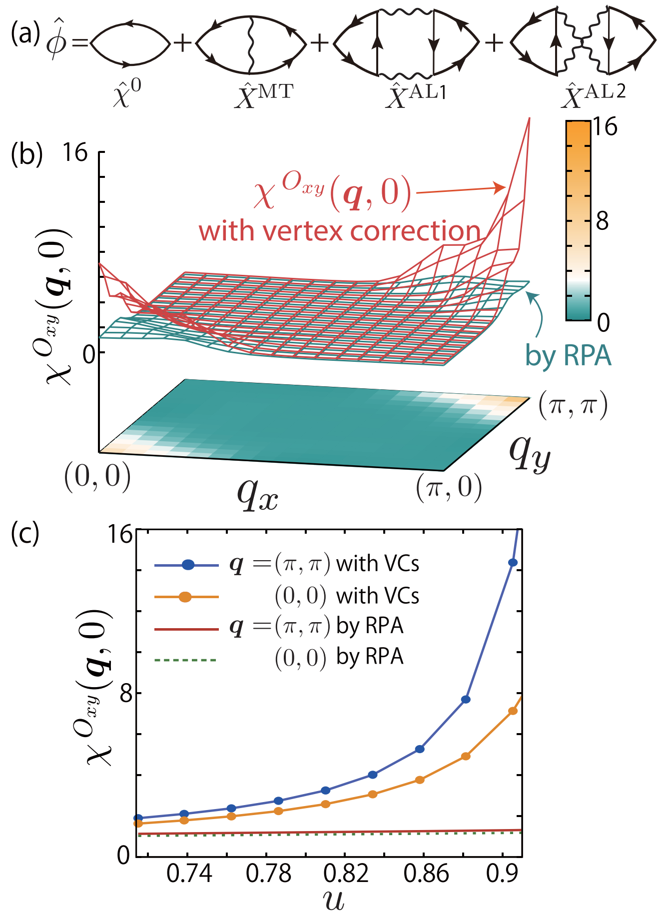

FIG. 3. (a) Diagrams of the irreducible susceptibility $\hat{\phi}$ with MT- and AL-VCs. (b) $\boldsymbol{q}$ dependence of $\chi^{O_{xy}}(\boldsymbol{q}, 0)$; $\alpha^{\Gamma_4^+} = 0.94$ with VCs. (c) u dependence of $\chi^{O_{xy}}(\boldsymbol{q}, 0)$ at $\boldsymbol{q} = \boldsymbol{Q}, \boldsymbol{0}$.

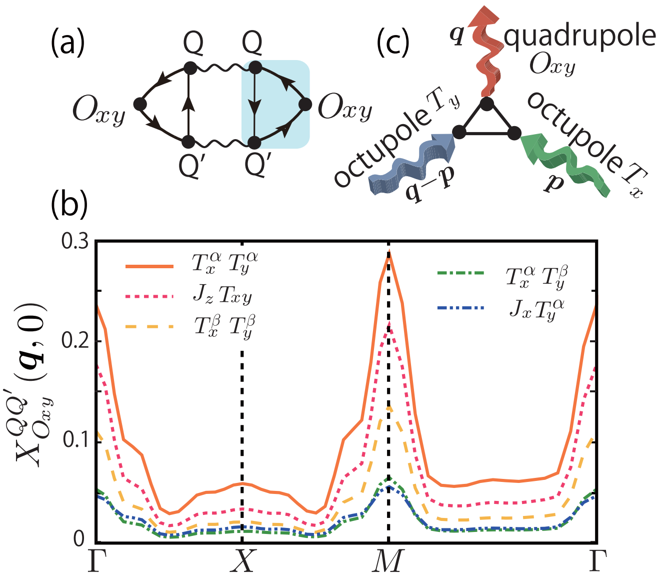

FIG. 4. (a) AL term $X_{O_{xy}}^{\mathrm{AL1},QQ'}$ given by (Q,Q')-channel fluctuations. (b) Obtained $X_{O_{xy}}^{QQ'}(\boldsymbol{q},0)$. (c) Quantum process of O_{xy} fluctuations driven by the interference between (T_x,T_y) fluctuations, which corresponds to the shaded area in (a). Note that $\chi^{O_{xy}} \neq \chi^{O_{xz(yz)}}$ in the present 2D model; see SM [39].

By following Ref. [27], we expand $\hat{V}(q)$ on the basis of the multipole operator as

$$\hat{V}(q) = \sum_{QQ'} v_q^{QQ'} \vec{Q}(\vec{Q}')^\dagger, \tag{10}$$

where the real coefficient $v_q^{QQ'}$ is uniquely determined [27]. From Eqs. (7), (9), and (10), the AL1 term due to (Q,Q')-channel fluctuations is given as

$$X_{O_{xy}}^{\mathrm{AL1},QQ'}(q) \equiv \frac{T}{2}\sum_p v_p^Q v_{p-q}^{Q'} \Lambda_{q,p}^{O_{xy}QQ'} \left(\Lambda_{\bar{q},\bar{p}}^{O_{xy}Q'Q}\right)^*, \tag{11}$$

where $v^Q \equiv v^{QQ}$ and $\Lambda_{q,p}^{O_{xy}QQ'}$ is defined as

$$\Lambda_{q,p}^{O_{xy}QQ'} \equiv \sum_\alpha (\vec{O}_{xy})_\alpha^* (\vec{Q}')^\dagger \hat{\Lambda}^\alpha(q,p)\vec{Q}. \tag{12}$$

The diagrammatic expression of Eq. (11) is shown in Fig. 4(a). Figure 4(b) shows the $\boldsymbol{q}$ dependence of $X_{O_{xy}}^{QQ'}(\boldsymbol{q},0)$ at $u = 0.91$. We find that the $(Q,Q') = (T_x^\alpha, T_y^\alpha), (J_z, T_{xyz}), (T_x^\beta, T_y^\beta)$ channels make the dominant contributions. Other terms not shown in Fig. 4(b) make a negligible contribution.

Figure 4(c) presents the quantum process of the O_{xy} quadrupole order driven by the interference between (T_x, T_y) fluctuations, which corresponds to $\Lambda^{O_{zx}T_xT_y}$ in Fig. 4(a). This process is realized when $\Lambda^{O_{zx}QQ'} \sim \mathrm{Tr}\{\hat{O}_{xy}\cdot\hat{Q}\cdot\hat{Q}'\} \neq 0$. Since $\Lambda^{QTT'} = 0$ for odd-rank Q, the AL-VC is unimportant for χ^J and χ^T [30].

Next, the $\boldsymbol{q}$ dependence of the AL-VC is given as $X_{O_{xy}}^{T_xT_y}(\boldsymbol{q}) \propto \sum_{\boldsymbol{p}} \chi^{T_x}(\boldsymbol{p})\chi^{T_y}(\boldsymbol{q}-\boldsymbol{p})$, which becomes large at $\boldsymbol{q} = \boldsymbol{Q}$ and $\boldsymbol{q} = \boldsymbol{0}$ since $\chi^{T_\mu}(\boldsymbol{p})$ has large peaks at $\boldsymbol{p} \sim \boldsymbol{Q}, \boldsymbol{0}$ shown in Fig. 2. Thus, antiferroquadrupole order in CeB_6 originates from the interference between ferro- and antiferromagnetic multipole fluctuations.

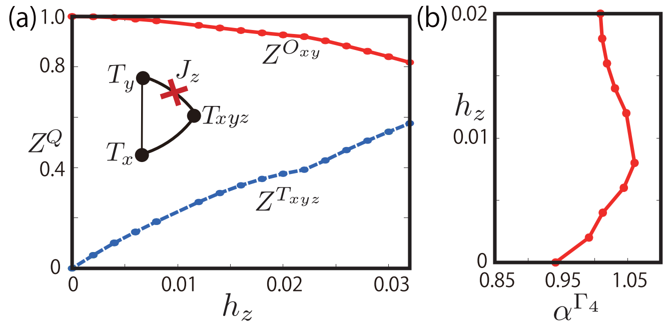

FIG. 5. (a) Form factor $(Z^{O_{xy}}, Z^{T_{xyz}})$ of the eigenvector for $\Gamma_4 = \{O_{xy}, T_{xyz}\}$ at $\boldsymbol{q} = \boldsymbol{Q}$ under h_z. Inset: h_z-linear term of the three-point vertex $\Lambda^{T_{xyz}T_xT_y}$ that gives large $\chi^{O_{xy}T_{xyz}}(\boldsymbol{q},0)$. (b) Stoner factor α^{Γ_4} as a function of h_z.

Finally, we discuss the field-induced octupole order, which has been studied intensively as a main issue of CeB_6 [13–16]. The Zeeman term under the magnetic field along the z axis is given as $\hat{H}_Z = h_z \sum_{L,M} (\hat{J}_z)_{L,M} f_{\boldsymbol{k}L}^\dagger f_{\boldsymbol{k}M}$. When $h_z \neq 0$, both O_{xy} and T_{xyz} belong to the same IR Γ_4 shown in Table I [13]. Therefore, a large quadrupole-octupole susceptibility $\chi^{O_{xy},T_{xyz}}(\boldsymbol{q},0)$ is induced in proportion to h_z. To verify this, we solve the eigenequation (4) for the IR Γ_4 under h_z, at the fixed magnetic Stoner factor in the RPA $\alpha^{\mathrm{mag}} = 0.8$ [44,45].

Figures 5(a) and 5(b) show the obtained eigenvector $\vec{w}^{\Gamma_4}(\boldsymbol{q}) = Z^{O_{xy}}(\boldsymbol{q})\vec{O}_{xy} + Z^{T_{xyz}}(\boldsymbol{q})\vec{T}_{xyz}$ ($|\vec{w}^{\Gamma_4}|^2 = 1$) and the Stoner factor α^{Γ_4} at $\boldsymbol{q} = \boldsymbol{Q}$, respectively, as functions of h_z. Here, α^{Γ_4} is the largest Stoner factor. The increment of α^{Γ_4} under h_z is consistent with the field enhancement of T_Q in CeB_6. (In contrast, T_N will be suppressed by a large O_{xz} moment.) Also, $Z^{T_{xyz}}$ increases linearly in h_z, due to the interference process under h_z shown in the inset of Fig. 5(b). $Z^{T_{xyz}}$ becomes comparable to $Z^{O_{xy}}$ under a small magnetic field $h_z \lesssim 0.03 \ll W_D^{qp}/10$. Since the ratio of the ordered momenta at T_Q is $M^{T_{xyz}}/M^{O_{xy}} = Z^{T_{xyz}}/Z^{O_{xy}}$, field-induced antiferro-T_{xyz} order is naturally explained.

In summary, we developed a multipole fluctuation theory by focusing on the AL-type VCs in HF systems, and applied the theory to the multipole order physics in CeB_6. Both ferro- and antiferromagnetic multipole fluctuations emerge in CeB_6 due to the nesting of Fermi surfaces, consistent with neutron experiments. Then, antiferro-O_{xy} order in CeB_6 at T_Q ($>T_N$) is derived from the interference between different magnetic multipole fluctuations, which is depicted in Fig. 4(c). We also explained the field-induced octupole order, which is a central issue of CeB_6. The discovered intermultipole coupling mechanism will be significant in other HF systems [46,47] and $4d, 5d$ transition metal compounds [48]. Although the analysis of AL-VC in three-dimensional PAM is very difficult, it is an important future problem.

We stress that the on-site quadrupole (O_{xy}) interaction on the Ce ion is about 60% of the dipole (J_μ) one as shown in Table II. Therefore, a quadrupole order cannot appear within the mean-field theory. In contrast, in the localized Ruderman-Kittel-Kasuya-Yosida (RKKY) model, the quadrupole interaction is as large as the dipole interaction [13,16,49]. Such a discrepancy between the itinerant picture and localized one, which is an important problem in HF systems, is partially resolved by considering the VCs as we discussed here.

We are grateful to S. Onari and Y. Yamakawa for useful discussions. This work has been supported by the Quantum Liquid Crystals No. JP19H05825 KAKENHI on Innovative Areas from JSPS of Japan, and JSPS KAKENHI (No. JP18J12852, JP18H01175).

[1] P. Coleman, *Handbook of Magnetism and Advanced Magnetic Materials* (Wiley, Hoboken, NJ, 2007), Vol. 1, pp. 95–148.
[2] T. Moriya and K. Ueda, Adv. Phys. **49**, 555 (2000).
[3] Y. Yanase, T. Jujo, T. Nomura, H. Ikeda, T. Hotta, and K. Yamada, Phys. Rep. **387**, 1 (2003).
[4] H. Kontani, Rep. Prog. Phys. **71**, 026501 (2008).
[5] P. Monthoux, D. Pines, and G. G. Lonzarich, Nature (London) **450**, 1177 (2007).
[6] D. Senechal and A.-M. S. Tremblay, Phys. Rev. Lett. **92**, 126401 (2004).
[7] P. Monthoux and D. J. Scalapino, Phys. Rev. Lett. **72**, 1874 (1994).
[8] T. Takimoto, T. Hotta, and K. Ueda, J. Phys.: Condens. Matter **15**, S2087 (2003).
[9] T. Fujita, M. Suzuki, T. Komatsubara, S. Kunii, T. Kasuya, and T. Ohtsuka, Solid State Commun. **35**, 569 (1980).
[10] S. Nakamura, T. Goto, S. Kunii, K. Iwashita, and A. Tamaki, J. Phys. Soc. Jpn. **63**, 623 (1994).
[11] M. Hiroi, S. Kobayashi, M. Sera, N. Kobayashi, and S. Kunii, J. Phys. Soc. Jpn. **66**, 1762 (1997).
[12] A. S. Cameron, G. Friemel, and D. S. Inosov, Rep. Prog. Phys. **79**, 066502 (2016).
[13] R. Shiina, S. Shiba, and P. Thalmeier, J. Phys. Soc. Jpn. **66**, 1741 (1997).
[14] O. Sakai, R. Shiina, H. Shiba, and P. Thalmeier, J. Phys. Soc. Jpn. **66**, 3005 (1997); **68**, 1364 (1999).
[15] P. Thalmeier, R. Shiina, H. Shiba, and O. Sakai, J. Phys. Soc. Jpn. **67**, 2363 (1998).
[16] H. Shiba, O. Sakai, and R. Shiina, J. Phys. Soc. Jpn. **68**, 1988 (1999).
[17] M. Sera and S. Kobayashi, J. Phys. Soc. Jpn. **68**, 1664 (1999).
[18] H. Kusunose and Y. Kuramoto, J. Phys. Soc. Jpn. **74**, 3139 (2005).
[19] K. Hanzawa, J. Phys. Soc. Jpn. **70**, 468 (2001).
[20] M. Neupane, N. Alidoust, I. Belopolski, G. Bian, S.-Y. Xu, D.-J. Kim, P. P. Shibayev, D. S. Sanchez, H. Zheng, T.-R. Chang, H.-T. Jeng, P. S. Riseborough, H. Lin, A. Bansil, T. Durakiewicz, Z. Fisk, and M. Z. Hasan, Phys. Rev. B **92**, 104420 (2015).
[21] A. Koitzsch, N. Heming, M. Knupfer, B. Buchner, P. Y. Portnichenko, A. V. Dukhnenko, N. Y. Shitsevalova, V. B. Filipov, L. L. Lev, V. N. Strocov, J. Ollivier, and D. S. Inosov, Nat. Commun. **7**, 10876 (2016).
[22] G. Friemel, Y. Li, A. V. Dukhnenko, N. Yu. Shitsevalova, N. E. Sluchanko, A. Ivanov, V. B. Filipov, B. Keimer, and D. S. Inosov, Nat. Commun. **3**, 830 (2012).
[23] H. Jang, G. Friemel, J. Ollivier, A. V. Dukhnenko, N. Yu. Shitsevalova, V. B. Filipov, B. Keimer, and D. S. Inosov, Nat. Mater. **13**, 682 (2014).
[24] A. Akbari and P. Thalmeier, Phys. Rev. Lett. **108**, 146403 (2012).
[25] M. Endo, S. Nakamura, T. Isshiki, N. Kimura, T. Nojima, H. Aoki, H. Harima, and S. Kunii, J. Phys. Soc. Jpn. **75**, 114704 (2006).
[26] H. Ikeda, M.-T. Suzuki, R. Arita, T. Takimoto, T. Shibauchi, and Y. Matsuda, Nat. Phys. **8**, 528 (2012).
[27] R. Tazai and H. Kontani, Phys. Rev. B **98**, 205107 (2018).
[28] S. Onari and H. Kontani, Phys. Rev. Lett. **109**, 137001 (2012).
[29] S. Onari, Y. Yamakawa, and H. Kontani, Phys. Rev. Lett. **116**, 227001 (2016).
[30] Y. Yamakawa, S. Onari, and H. Kontani, Phys. Rev. X **6**, 021032 (2016).
[31] M. Tsuchiizu, Y. Ohno, S. Onari, and H. Kontani, Phys. Rev. Lett. **111**, 057003 (2013).
[32] M. Tsuchiizu, Y. Yamakawa, S. Onari, Y. Ohno, and H. Kontani, Phys. Rev. B **91**, 155103 (2015).
[33] M. Tsuchiizu, Y. Yamakawa, and H. Kontani, Phys. Rev. B **93**, 155148 (2016).
[34] R. Tazai, Y. Yamakawa, M. Tsuchiizu, and H. Kontani, Phys. Rev. B **94**, 115155 (2016).
[35] M. Tsuchiizu, K. Kawaguchi, Y. Yamakawa, and H. Kontani, Phys. Rev. B **97**, 165131 (2018).
[36] R.-Q. Xing, L. Classen, and A. V. Chubukov, Phys. Rev. B **98**, 041108(R) (2018).
[37] U. Karahasanovic, F. Kretzschmar, T. Bohm, R. Hackl, I. Paul, Y. Gallais, and J. Schmalian, Phys. Rev. B **92**, 075134 (2015).
[38] R. Tazai, Y. Yamakawa, M. Tsuchiizu, and H. Kontani, J. Phys. Soc. Jpn. **86**, 073703 (2017).
[39] See Supplemental Material at http://link.aps.org/supplemental/10.1103/PhysRevB.100.241103 for model Hamiltoninan, multipole operator, and multipole fluctuations.
[40] K. Takegahara, Y. Aoki, and A. Yanase, J. Phys. C **13**, 583 (1980).
[41] Y. Kubo and S. Asano, Phys. Rev. B **39**, 8822 (1989).
[42] A. Hasegawa and A. Yanase, J. Phys. F **7**, L7 (1977).
[43] At $T \sim T_Q$, $\chi^{J_\mu}(\boldsymbol{q}, \omega)$ at $\boldsymbol{q} = \boldsymbol{Q}, \boldsymbol{0}$ is much larger than that at the magnetic order wave vector $\boldsymbol{Q}_N = (\pi/2, \pi/2, 0)$ below T_N according to Ref. [23].
[44] We adjust u to keep $\alpha^{\rm mag}$ constant, since $\alpha^{\rm mag}$ decreases with h_z for fixed u in the RPA. In the fluctuation exchange (FLEX) approximation, $\alpha^{\rm mag}$ increases with h_z due to the negative feedback effect between spin fluctuations and self-energy [45].
[45] K. Sakurazawa, H. Kontani, and T. Saso, J. Phys. Soc. Jpn. **74**, 271 (2005).
[46] T. Takimoto and P. Thalmeier, Phys. Rev. B **77**, 045105 (2008).
[47] K. Kubo and T. Hotta, Phys. Rev. B **71**, 140404(R) (2005).
[48] S. Hayami, Y. Yanagi, H. Kusunose, and Y. Motome, Phys. Rev. Lett. **122**, 147602 (2019).
[49] T. Yamada and K. Hanzawa, J. Phys. Soc. Jpn. **88**, 084703 (2019).